



CHORUS

This is the accepted manuscript made available via CHORUS. The article has been published as:

Hard three-loop corrections to hyperfine splitting in positronium and muonium

Michael I. Eides and Valery A. Shelyuto

Phys. Rev. D **92**, 013010 — Published 17 July 2015

DOI: [10.1103/PhysRevD.92.013010](https://doi.org/10.1103/PhysRevD.92.013010)

Hard Three-Loop Corrections to Hyperfine Splitting in Positronium and Muonium

Michael I. Eides*

*Department of Physics and Astronomy,
University of Kentucky, Lexington, KY 40506, USA*

Valery A. Shelyuto†

D. I. Mendeleev Institute for Metrology, St.Petersburg 190005, Russia

Abstract

We consider hard three-loop corrections to hyperfine splitting in muonium and positronium generated by the diagrams with closed electron loops. There are six gauge-invariant sets of such diagrams that generate corrections of order $m\alpha^7$. The contributions of these diagrams are calculated for an arbitrary electron-muon mass ratio without expansion in the small mass ratio. We obtain the formulae for contributions to hyperfine splitting that in the case of small mass ratio describe corrections for muonium and in the case of equal masses describe corrections for positronium. First few terms of the expansion of hard corrections in the small mass ratio were earlier calculated for muonium analytically. We check numerically that the new results coincide with the sum of the known terms of the expansion in the case of small mass ratio. In the case of equal masses we obtain hard nonlogarithmic corrections of order $m\alpha^7$ to hyperfine splitting in positronium.

* Also at the Petersburg Nuclear Physics Institute, Gatchina, St.Petersburg 188300, Russia; Email address:

eides@pa.uky.edu, eides@thd.pnpi.spb.ru

† Email address: shelyuto@vniim.ru

I. INTRODUCTION

For many years hyperfine splitting (HFS) in muonium and positronium remains an active field of experimental and theoretical research. Results of highly accurate HFS measurements can be compared with the theoretical predictions of quantum electrodynamics obtained from the first principles without any adjustable parameters. Both experiment and theory have achieved very high accuracy. The experimental errors for HFS in muonium are now in the interval 16-51 Hz [1, 2], and a new measurement with the goal to reduce the error to about 10 Hz or to a few parts in 10^9 is now planned at J-PARC [3, 4]. Current theoretical uncertainty of HFS in muonium is about 70-100 Hz, see, e.g., reviews in [5–7]. Recent theoretical work on HFS in muonium concentrated on calculation of radiative-recoil corrections of order $\alpha^3(m/M)E_F$ that arise from the three-loop diagrams with closed electron and muon loops [8–12]. The goal of this work is to reduce the theoretical error below 10 Hz.

The hyperfine splitting in positronium is measured with the error bars at the level of 1-2 MHz [13–16]. There is a discrepancy about three standard deviations between the results of old and new experiments. New measurement of the positronium HFS splitting is now planned at J-PARC [17]. All theoretical contributions to HFS in positronium of order $m\alpha^6$ and logarithmic corrections of order $m\alpha^7$ are already known, see, e.g., reviews in [18–20]. A new stage in the theory of positronium HFS was opened in [19] where the one-photon annihilation contribution of order $m\alpha^7$ was calculated. This paper was soon followed by the works of Adkins and collaborators [20, 21], who calculated contributions of the light-by-light scattering insertion in the scattering and annihilation channels.

Hard nonlogarithmic contributions to HFS in positronium of order $m\alpha^7$ are similar to the radiative and radiative-recoil corrections to HFS in muonium of orders $\alpha^2(Z\alpha)E_F$ and $\alpha^2(Z\alpha)(m/M)E_F$, respectively. We have calculated these corrections in muonium some time ago [8–12]. The corrections in muonium are power series in the electron-muon mass ratio with the coefficients enhanced by large logarithms of this mass ratio. The goal of the old work on muonium was to calculate the coefficients in this expansion, at least the factors before the logarithms, analytically. In the case of positronium the masses are equal and the hard corrections of order $m\alpha^7$ are pure numbers. We apply the approach developed for muonium to positronium. We consider an electromagnetically bound system of two particles with arbitrary masses M and m , and obtain general expressions for the hard corrections to HFS

of order $m\alpha^7$ without expansion in the mass ratio of the constituents. We check numerically that in the case of a small mass ratio these formulae reproduce with high accuracy the sum of all already known terms in the expansion in the small mass ratio for muonium. We use the general expressions for the case of equal masses and calculate all hard three-loop contributions to HFS in positronium of order $m\alpha^7$ that are due to the diagrams with closed electron loops. The results of these calculations were reported in the rapid communication [22]. Below we present the details of the calculations in the general case of arbitrary mass ratio and in the special case of equal masses, for positronium.

II. CALCULATIONS

We start with the infrared divergent contribution to HFS in muonium generated by the two-photon exchange diagrams in Fig. 1 calculated in the scattering approximation

$$\begin{aligned}\Delta E &= -\frac{Z\alpha}{\pi}E_F\frac{3mM}{16}\int\frac{d^4q}{i\pi^2q^4}L_{e,skel}^{\alpha\beta}(q)L_{\mu,skel,\alpha\beta}(-q) \\ &= -\frac{Z\alpha}{\pi}E_F(2mM)\int\frac{d^4q}{i\pi^2q^4}(2q^2+q_0^2)L_{skel}^{(e)}(q)L_{skel}^{(\mu)}(-q),\end{aligned}\tag{1}$$

where

$$L_{e,skel}^{\alpha\beta}(q)\equiv-\frac{2q^2}{q^4-4m^2q_0^2}\gamma^\mu\hat{q}\gamma^\nu=2L_{skel}^{(e)}\gamma^\mu\hat{q}\gamma^\nu\tag{2}$$

is the forward electron Compton scattering amplitude in the tree approximation (the skeleton electron-line factor), and $L_{\mu,skel}^{\alpha\beta}(q)$ is a similar amplitude for the muon. The Fermi energy is defined as $E_F=(8/3)(Z\alpha)^4m_r^3/(mM)$, where $m_r=mM/(m+M)$ is the reduced mass. In the case of equal masses, $M=m$, the Fermi energy E_F turns into the leading nonannihilation contribution to HFS in positronium $E_F^{\text{Ps}}=m\alpha^4/3$. The external electron and muon lines in the diagrams in Fig. 1 are on the mass shell and carry zero spatial momenta. In the second line in Eq. (1) we calculated projection of the matrix elements on HFS.



FIG. 1. Diagrams with two-photon exchanges

After the Wick rotation and transition to four-dimensional spherical coordinates ($q_0 = q \cos \theta$, $|\mathbf{q}| = q \sin \theta$) we obtain

$$\begin{aligned} \Delta E &= \frac{Z\alpha}{\pi} E_F \frac{4mM}{\pi} \int_0^\pi d\theta \sin^2 \theta \int_0^\infty dq^2 (2 + \cos^2 \theta) L_{skel}^{(e)} L_{skel}^{(\mu)} \\ &= \frac{Z\alpha}{\pi} E_F \frac{4mM}{\pi} \int_0^\pi d\theta \sin^2 \theta \int_0^\infty dq^2 \frac{2 + \cos^2 \theta}{(q^2 + 4m^2 \cos^2 \theta)(q^2 + 4M^2 \cos^2 \theta)} \\ &\equiv \frac{Z\alpha}{\pi} E_F \frac{mM}{M^2 - m^2} \int_0^\infty dq^2 f_\mu(q), \end{aligned} \quad (3)$$

where at the last step we rescaled the integration momentum $q \rightarrow qm$. The dimensionless weight function $f_\mu(q)$ in terms of an auxiliary function

$$f(q) = -\frac{1}{4} + \frac{\sqrt{q^2 + 4}}{4q} - \frac{2\sqrt{q^2 + 4}}{q^3} \quad (4)$$

has the form

$$f_\mu(q) = f(q) - 4\mu^2 f(2\mu q), \quad (5)$$

where $\mu = m/(2M)$.

In the case of positronium $M \rightarrow m$ and the weight function simplifies

$$\frac{mM}{M^2 - m^2} f_\mu(q) \Big|_{M \rightarrow m} \rightarrow \frac{16 + 2q^2 + q^4 - q^3 \sqrt{q^2 + 4}}{4q^3 \sqrt{q^2 + 4}} \equiv f_p(q). \quad (6)$$

Respectively, the skeleton integral in Eq. (3) in the case of positronium turns into

$$\begin{aligned} \Delta E &= \frac{\alpha}{\pi} E_F^{\text{Ps}} \frac{4m^2}{\pi} \int_0^\pi d\theta \sin^2 \theta \int_0^\infty dq^2 L_{e,skel}^2 (2 + \cos^2 \theta) \\ &= \frac{\alpha}{\pi} E_F^{\text{Ps}} \frac{4m^2}{\pi} \int_0^\pi d\theta \sin^2 \theta \int_0^\infty dq^2 \frac{2 + \cos^2 \theta}{(q^2 + 4m^2 \cos^2 \theta)^2} \equiv \frac{\alpha}{\pi} E_F^{\text{Ps}} \int_0^\infty dq^2 f_p(q). \end{aligned} \quad (7)$$

The integrals in Eq. (3) and Eq. (7) are sums of an infrared linearly divergent integral and a finite one. In a more accurate approximation (with the off mass shell external fermion lines) the linear divergence is cutoff at the characteristic atomic scale $\lambda \sim m\alpha$ and generates an extra factor $m/\lambda \sim 1/\alpha$. As a result the infrared divergent term turns into a contribution of order E_F that is of lower order in α . Therefore the uncertainty connected with the lack of knowledge of the precise value of the infrared cutoff is hidden in the contribution to HFS that is of lower order in α and that anyway cannot be calculated in the scattering

approximation. The remaining finite part of the integral originates at hard integration momenta $\sim m$ (or in the interval from m to M in the case of unequal masses) and generates a contribution of order αE_F . In the case of unequal masses, for muonium, the linearly infrared divergent contribution turns into the leading nonrecoil Fermi contribution E_F to HFS, while the finite part generates the leading recoil correction of order $\alpha(m/M)E_F$, see, e.g., [5, 6]. Let us emphasize that due to the linear (as opposed to logarithmic) nature of the apparent divergence it leaves no finite remnant of order αE_F and should be simply thrown away. No need in matching of high and low integration momenta arises. This feature should be contrasted with the case of a logarithmic infrared divergence when the cutoff at the atomic scale λ produces a logarithm $\ln(m/\lambda) \sim \ln(1/\alpha)$ and uncertainty in the precise value of the infrared cutoff generates uncontrolled nonlogarithmic contributions to HFS of the same order in α as the logarithmic term. This effect clearly indicates that an accurate matching of hard and soft momenta contributions is mandatory in the case of logarithmic infrared divergences. A rigorous formal proof of these features of linear and logarithmic infrared divergences can be found, e.g. in [23, 24].

Six gauge-invariant sets of diagrams in Figs. 2 - 4 and in Figs. 6 - 8 generate hard radiative corrections of order $m\alpha^7$ that are due to the graphs with closed electron loops¹. All these diagrams can be interpreted as the results of radiative insertions in the skeleton diagrams with two-photon exchanges in Fig. 1. It is well known that insertion of radiative corrections suppresses the low integration momentum region, see, e.g., [5, 6, 23]. Hence, all diagrams in Figs. 2 - 4 and in Figs. 6 - 8 are infrared convergent². Moreover, the characteristic integration momenta in these diagrams are hard (of order $\sim m$ or in the interval from m to M in the case of unequal masses) and are much larger than the atomic momenta of order $\sim m\alpha$, what justifies validity of the scattering approximation for their calculation. This is exactly the approximation we used above in calculation of the contribution of the skeleton diagrams in Fig. 1, and all corrections calculated below are obtained by some modifications of the basic integrals in Eq. (3) and Eq. (7).

¹ All gauge-invariant sets of diagrams include the graphs with the crossed exchanged photons that we do not show explicitly.

² Linearly infrared divergent contributions due to the anomalous magnetic moment should be subtracted from radiative corrections in Figs. 6 and Fig. 8, see more on this below.

A. Analytic Results for One- and Two-Loop Polarization Insertions in the Exchanged Photons

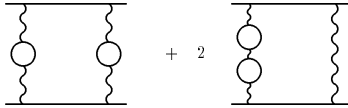


FIG. 2. Diagrams with two one-loop polarization insertions

Consider first the diagrams in Fig. 2 with two one-loop polarization loops. Insertion of a polarization operator in a photon line with momentum q (all momenta below are measured in units of the electron mass) reduces to the replacement in the photon propagator

$$\frac{1}{q^2} \rightarrow \frac{\alpha}{\pi} I_1(q), \quad (8)$$

where $(\alpha/\pi)I_1(q)$ is the well known representation of the one-loop vacuum polarization [25]

$$\frac{\alpha}{\pi} I_1(q) = \frac{\alpha}{\pi} \int_0^1 dv \frac{v^2(1 - \frac{v^2}{3})}{1 - v^2} \frac{1}{q^2 + \frac{4}{1-v^2}}. \quad (9)$$

We see that a photon line that carries a polarization loop has a natural interpretation as a propagator of a massive photon with mass squared $\lambda^2 = 4/(1 - v^2)$. According to Eq. (9) this propagator should be integrated over v with the weight $(\alpha/\pi)v^2(1 - v^2/3)/(1 - v^2)$.

The contribution of the diagrams in Fig. 2 is obtained by insertion of the one-loop photon polarization squared $(\alpha/\pi)^2 q^4 I_1^2(q)$ in the integrands in Eq. (3) and Eq. (7). Due to nonsingular behavior of the polarization operator at $q^2 \rightarrow 0$ we obtain convergent integrals where the effective integration momenta are hard, of order $\sim m$ (or in the interval from $\sim m$ to M in the case of unequal masses). Then in the general case of unequal masses the contribution to HFS has the form

$$\Delta E = 3 \frac{\alpha^2(Z\alpha)}{\pi^3} E_F \frac{mM}{M^2 - m^2} \int_0^\infty dq^2 f_\mu(q) q^4 I_1^2(q), \quad (10)$$

where the factor 3 before the integral has the combinatorial origin. We checked numerically that in the small mass ratio limit this integral reproduces the sum of all known analytically terms [26, 27] of the expansion of this contribution in the small mass ratio.

In the case of positronium the integral in Eq. (10) reduces to (compare Eq. (7))

$$\Delta E_1 = 3 \frac{\alpha^3}{\pi^3} E_F^{\text{Ps}} \int_0^\infty dq^2 f_p(q) q^4 I_1^2(q), \quad (11)$$

and after computation we obtain the contribution to HFS of the diagrams with two one-loop polarization insertions in Fig. 2

$$\Delta E_1 = \left(\frac{6\pi^2}{35} - \frac{8}{9} \right) \frac{\alpha^3}{\pi^3} E_F^{\text{Ps}} = 0.803\,043\,294 \frac{\alpha^3}{\pi^3} E_F^{\text{Ps}}. \quad (12)$$

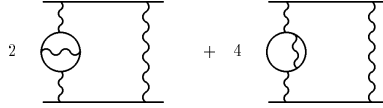


FIG. 3. Diagrams with two-loop polarization insertions

The contribution of the two-loop vacuum polarization in Fig. 3 can be obtained by the insertion of the two-loop photon polarization $(\alpha^2/\pi^2)q^2 I_2(q)$ [25, 28] in the integrands in Eq. (3) and Eq. (7)

$$\begin{aligned} \left(\frac{\alpha}{\pi}\right)^2 I_2(q) = & \frac{2}{3} \left(\frac{\alpha}{\pi}\right)^2 \int_0^1 dv \frac{v}{4 + q^2(1 - v^2)} \left\{ (3 - v^2)(1 + v^2) \left[\text{Li}_2 \left(-\frac{1 - v}{1 + v} \right) \right. \right. \\ & + 2\text{Li}_2 \left(\frac{1 - v}{1 + v} \right) + \frac{3}{2} \ln \frac{1 + v}{1 - v} \ln \frac{1 + v}{2} - \ln \frac{1 + v}{1 - v} \ln v \left. \right] \\ & + \left[\frac{11}{16} (3 - v^2)(1 + v^2) + \frac{v^4}{4} \right] \ln \frac{1 + v}{1 - v} \\ & \left. + \left[\frac{3}{2} v(3 - v^2) \ln \frac{1 - v^2}{4} - 2v(3 - v^2) \ln v \right] + \frac{3}{8} v(5 - 3v^2) \right\}, \end{aligned} \quad (13)$$

where the dilogarithm is defined as $\text{Li}_2(z) = -\int_0^1 dt \ln(1 - zt)/t$.

In the case of unequal masses the integral for the contribution to HFS of the diagrams with the two-loop polarization in Fig. 3 loop has the form

$$\Delta E = 2 \frac{\alpha^2(Z\alpha)}{\pi^3} E_F \frac{mM}{M^2 - m^2} \int_0^\infty dq^2 f_\mu(q) q^2 I_2(q), \quad (14)$$

where the factor 2 before the integral is due to combinatorics. Again, due to nonsingular behavior of the two-loop polarization at small $q^2 \rightarrow 0$ the integral in Eq. (14) is convergent, and typical integration momenta are hard, in the interval from m to M . We checked numerically that in the small mass ratio case the integral in Eq. (14) coincides with the sum

of the known terms [26, 27] of the expansion of this contribution to HFS in the small mass ratio.

In the case of equal masses, for positronium, the contribution to HFS of the diagrams in Fig. 3 reduces to the integral

$$\Delta E_2 = 2 \frac{\alpha^3}{\pi^3} E_F^{\text{Ps}} \int_0^\infty dq^2 f_p(q) q^2 I_2(q). \quad (15)$$

This integral admits an analytic calculation, and we obtain

$$\Delta E_2 = \left[-\frac{217}{30} \zeta(3) + \frac{28\pi^2}{15} \ln 2 + \frac{\pi^2}{675} + \frac{403}{360} \right] \frac{\alpha^3}{\pi^3} E_F^{\text{Ps}} = 5.209\,219\,614 \frac{\alpha^3}{\pi^3} E_F^{\text{Ps}}. \quad (16)$$

B. One-Loop Electron Factor and One-Loop Polarization Insertion in the Exchanged Photon

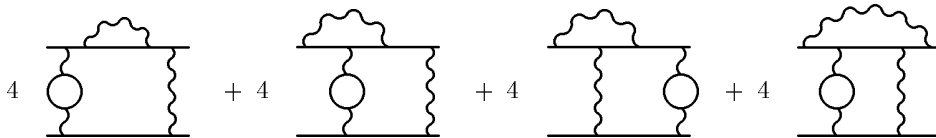


FIG. 4. Diagrams with one-loop polarization and radiative photon insertions

The diagrams in Fig. 4 are obtained from the skeleton diagrams in Fig. 1 by one-loop radiative insertions in one of the exchanged photons and one of the fermion lines³. To describe these radiative insertions it is convenient to introduce the one-loop electron factor that is defined as a gauge invariant sum of the diagrams in Fig. 5 where the external electron lines are on-shell and carry zero spatial momenta (plus the diagrams with the exchanged external photon vertices). Physically the electron factor is a sum of one-loop corrections to the spin-dependent amplitude of the virtual forward Compton scattering.

The gauge invariant electron factor $\tilde{L}_{\mu\nu}$ can be written as a sum of two gauge invariant terms $\tilde{L}_{\mu\nu} = L_{\mu\nu} + L_{\mu\nu}^{(a)}$, where the term $L_{\mu\nu}^{(a)}$ is the contribution of the anomalous magnetic moment (for more details see, e.g., [29, 30]). The multiloop electron factors also can be written as sums of two gauge invariant terms. Representation of the electron factor in the

³ Multiplicity factors in these diagrams correspond to the case of positronium, not muonium.

form of a sum of two gauge invariant terms is convenient for calculations because these terms have different behavior at low virtual photon momenta. According to the generalized low-energy theorem (see, e.g., [5, 6]) all terms linear in the small photon momentum q are due to the term $L_{\mu\nu}^{(a)}$, while the term $L_{\mu\nu}$ decreases at least as q^2 at small q^2 . This different low-energy behavior determines the structure of the integrals for the contributions to hyperfine splitting. In the case of the diagrams in Fig. 6 and in Fig. 8 the contributions to HFS generated by the term $L_{\mu\nu}^{(a)}$ are of lower order in α than the apparent order of a diagram. Technically presence of the previous order contribution reveals itself as a linear infrared divergence of an integral calculated in the scattering approximation.

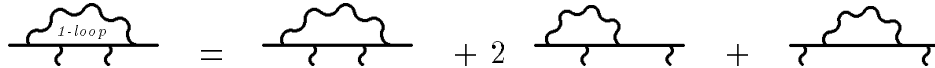


FIG. 5. One-loop fermion factor

In the diagrams in Fig. 4 the skeleton fermion line in Fig. 1 is effectively replaced by the one-loop fermion factor $\tilde{L}_{\mu\nu}$ in Fig. 5, what can be described by the substitution

$$L_{e,skel}^{\mu\nu}(q) \rightarrow \tilde{L}^{\mu\nu}(q) = 2\frac{\alpha}{4\pi} \left\{ \gamma^\mu \hat{q} \gamma^\nu \tilde{L}_I(q^2, q_0^2) + q_0 \left[\gamma^\mu \gamma^\nu - \frac{q^\mu \hat{q} \gamma^\nu + \gamma^\mu \hat{q} q^\nu}{q^2} \right] \tilde{L}_{II}(q^2, q_0^2) \right\}. \quad (17)$$

where $\tilde{L}_{I(II)}$ are scalar form factors. The scalar form factors $\tilde{L}_{I(II)}$ have the form

$$\tilde{L}_I = L_I + L_A, \quad \tilde{L}_{II} = L_{II} - L_A, \quad (18)$$

where the scalar form factors $L_{I(II)}$ and L_A correspond to $L_{\mu\nu}$ and $L_{\mu\nu}^{(a)}$, respectively. The factor 2 before the braces arises because we normalize the scalar form factors like the skeleton one in Eq. (2), and the factor $\alpha/(4\pi)$ is due to the one-loop integration in the fermion factor.

The one-loop electron factor $L_{\mu\nu}$ with the subtracted contribution of the anomalous magnetic moment enters calculations of the two-loop radiative-recoil corrections to HFS in muonium, and we had derived an explicit integral representations for the respective scalar form factors $L_{I(II)}$ long time ago [31–33]. After the Wick rotation, rescaling of the integration momentum $q \rightarrow qm$, and transition to the four-dimensional spherical coordinates the form factors can be written as

TABLE I. Coefficients in the Electron-Line Factor

c_1	$\frac{16}{y(1-y)^3} [(1-x)(x-3y) - 2y \ln x]$
c_2	$\frac{4}{y(1-y)^3} \left[-(1-x) \left(x - y - \frac{2y^2}{x} \right) + 2 \left(x - 4y + \frac{4y^2}{x} \right) \ln x \right]$
c_3	$\frac{1}{y(1-y)^2} \left[1 - 6x - 2x^2 - \frac{y}{x} \left(26 - \frac{6y}{x} - 37x - 2x^2 + 12xy + 16 \ln x \right) \right]$
c_4	$\frac{1}{y(1-y)^2} (2x - 4x^2 - 5y + 7xy)$
c_5	$\frac{1}{y(1-y)^2} (6x - 3x^2 - 8y + 2xy)$
c_6	$-b^2 \frac{x-y}{x^2}$
c_7	$2 \frac{1-x}{x}$

$$\begin{aligned}
 L_{\text{I}}(q^2, \cos^2 \theta) &= \int_0^1 dx \int_0^x dy \left\{ \frac{(q^2 + a^2) [(q^2 + a^2)^2 - 12b^2 q^2 \cos^2 \theta]}{[(q^2 + a^2)^2 + 4b^2 q^2 \cos^2 \theta]^3} (c_1 q^2 \sin^2 \theta + c_2 q^4) \right. \\
 &\quad \left. - \frac{(q^2 + a^2)^2 - 4b^2 q^2 \cos^2 \theta}{[(q^2 + a^2)^2 + 4b^2 q^2 \cos^2 \theta]^2} c_3 q^2 + \frac{(q^2 + a^2) 4b q^2 \cos^2 \theta}{[(q^2 + a^2)^2 + 4b^2 q^2 \cos^2 \theta]^2} 2c_4 \right\}, \\
 L_{\text{II}}(q^2, \cos^2 \theta) &= \int_0^1 dx \int_0^x dy \left\{ \frac{(q^2 + a^2) 4b}{[(q^2 + a^2)^2 + 4b^2 q^2 \cos^2 \theta]^2} c_5 q^2 \right. \\
 &\quad \left. - \frac{(q^2 + a^2)^2 - 4b^2 q^2 \cos^2 \theta}{[(q^2 + a^2)^2 + 4b^2 q^2 \cos^2 \theta]^2} 2c_6 q^2 + \frac{2b}{(q^2 + a^2)^2 + 4b^2 q^2 \cos^2 \theta} c_7 q^2 \right\},
 \end{aligned} \tag{19}$$

where $a^2 = x^2/y(1-y)$, $b = (1-x)/(1-y)$, and the coefficient functions c_i are collected in Table I.

The scalar form factor L_A is proportional to the respective skeleton form factor L_{skel} in Eq. (2). After the Wick rotation and in terms of the dimensionless integration momentum q it has the form

$$L_A = \frac{2}{q^2 + 4 \cos^2 \theta} = 2L_{skel}. \tag{20}$$

In the case of unequal masses an analytic expression for the contribution to HFS of the diagrams in Fig. 4 is obtained by modification of the skeleton integral in Eq. (3). First, we replace the skeleton factor in the integrand

$$(2 + \cos^2 \theta) L_{skel}^{(e)} \rightarrow \frac{\alpha}{4\pi} \left[(2 + \cos^2 \theta) \tilde{L}_{\text{I}} - 3 \cos^2 \theta \tilde{L}_{\text{II}} \right]. \tag{21}$$

The factor $\alpha/(4\pi)$ comes from the substitution in Eq. (17), and the term with \tilde{L}_{II} arises because the one-loop electron factor in Eq. (17) contains an additional spinor structure in comparison with the skeleton one in Eq. (2).

Second, we need to account for the polarization loops in Fig. 4 and insert the term $2q^2 I_1(q)$ in the integrand in Eq. (7). The factor 2 is due to two ways to insert the polarization operator in one of the exchanged photons. The polarization operator $q^2 I_1(q)$ decreases like q^2 at small q , and we obtain an infrared convergent integral with hard characteristic integration momenta of order m (or in the interval from m to M in the case of unequal masses). Due to suppression of the small integration momenta the anomalous magnetic moment in the diagrams in Fig. 4 gives contribution on par with the other terms in the one-loop electron factor $\tilde{L}^{\mu\nu}(q)$.

Then the contribution to HFS of the diagrams in Fig. 4 in the case of unequal masses has the form

$$\Delta E = \frac{\alpha^2(Z\alpha)}{\pi^3} E_F \frac{M}{m} \frac{2}{\pi} \int_0^\infty dq^2 q^2 I_1(q) \int_0^\pi d\theta \sin^2 \theta L_{skel}^{(\mu)} \left[(2 + \cos^2 \theta) \tilde{L}_{\text{I}} - 3 \cos^2 \theta \tilde{L}_{\text{II}} \right]. \quad (22)$$

The leading terms of the expansion of the contribution to HFS in Eq. (22) in the small mass ratio are already known for some time [26, 33, 34]

$$\Delta E = \frac{\alpha^2(Z\alpha)}{\pi^3} E_F \left[\pi^2 \left(-\frac{4}{3} \ln^2 \frac{1 + \sqrt{5}}{2} - \frac{20}{9} \sqrt{5} \ln \frac{1 + \sqrt{5}}{2} - \frac{64}{45} \ln 2 + \frac{\pi^2}{9} + \frac{3}{8} + \frac{1043}{675} \right) + \frac{m}{M} \left(\frac{5}{2} \ln^2 \frac{M}{m} + \frac{10}{3} \ln \frac{M}{m} + 11.41788 \right) \right]. \quad (23)$$

We have checked numerically that the integral in Eq. (22) coincides with this analytical result in the case of small mass ratio.

In the case of equal masses there is an extra factor 2 before the diagrams in Fig. 4. This factor arises because now there are two ways to insert the fermion factor in one of the lepton lines. Hence, the respective contribution to HFS is described by the doubled integral in Eq. (22) at $M = m$. Then we obtain the contribution of the diagrams in Fig. 4 to HFS in positronium in the form

$$\begin{aligned}
\Delta E_3 &= \frac{\alpha^3}{\pi^3} E_F^{Ps} \frac{4}{\pi} \int_0^\infty dq^2 q^2 I_1(q) \int_0^\pi d\theta \sin^2 \theta L_{skel} \left[(2 + \cos^2 \theta) \tilde{L}_I - 3 \cos^2 \theta \tilde{L}_{II} \right] \\
&= -1.287\,09 \text{ (1)} \frac{\alpha^3}{\pi^3} E_F^{Ps}.
\end{aligned}
\tag{24}$$

C. One-Loop Polarization Insertion in the Electron Factor

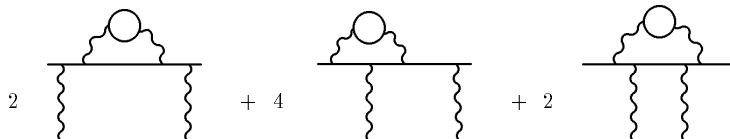


FIG. 6. Diagrams with one-loop polarization insertions in radiative photons

Consider now the diagrams in Fig. 6 with the one-loop polarization insertions in the radiative photon⁴. Effectively these diagrams contain a massive radiative photon, see Eq. (8) and Eq. (9). In principle, the respective electron factor can be obtained from the one-loop electron factor in Eq. (17) by restoring the radiative photon mass squared $\lambda^2 = 4m^2/(1 - v^2)$, followed by integration over v with the weight $(\alpha/\pi)v^2(1 - v^2/3)/(1 - v^2)$. However, the relatively compact expression in Eq. (17) is a result of numerous cancellations in the integrand between the contributions from different diagrams in Fig. 5, and technically it is much easier to start calculation of the two-loop electron factor in Fig. 6 from scratch. We consider this electron factor as a sum of the contributions corresponding to the separate diagrams in Fig. 6 with the self-energy, vertex and spanning photon insertions in the electron line. Each of these terms is calculated as a one-loop diagrams with a massive photon and then integrated over the auxiliary parameter v as we just explained.

The only subtlety in further calculations is connected with the diagrams with the vertex correction in Fig. 6. All entries in the two-loop fermion factor except the two-loop anomalous magnetic moment carry at least one extra power of q^2 at $q^2 \rightarrow 0$ in comparison with the skeleton electron factor. One can separate the contribution to the two-loop anomalous magnetic moment from the two-loop vertex in the second diagram in Fig. 6 in a gauge invariant way, like we separated the one-loop anomalous magnetic moment from the one-loop electron factor $L_{\mu\nu}$ above. The two-loop anomalous magnetic moment term in the

⁴ Multiplicity factors in these diagrams correspond to the case of positronium, not muonium.

second diagram in Fig. 6 generates a linearly infrared divergent contribution to HFS. This linear infrared divergence that is cutoff at the characteristic atomic scale $\sim m\alpha$ indicates that the anomalous magnetic moment generates a contribution to HFS of the previous order in α . This correction of order $m\alpha^6$ is already accounted for in earlier calculations and we should simply delete the apparently divergent term that generates it. To get rid of the spurious divergence we subtract the gauge invariant term with the two-loop anomalous magnetic moment from the two-loop electron vertex in Fig. 6. The subtracted two-loop electron factor in Fig. 6 can be written in terms of scalar two-loop form factors $L_{I,II}^{(2)}$

$$L_{I,II}^{(2)} = L_{I,II}^{(2,\Sigma)} + 2L_{I,II}^{(2,\Lambda)} + L_{I,II}^{(2,\Xi)} \quad (25)$$

similar to the one-loop form factors $L_{I,II}$ in Eq. (18). Unlike the one-loop form factors $\tilde{L}_{I,II}$ in Eq. (17) these two-loop form factors do not include contributions of the anomalous magnetic moment.

In terms of the scalar form factors in Eq. (25) the contribution to HFS of the diagrams in Fig. 6 in the general case has the form

$$\Delta E = \frac{\alpha^2(Z\alpha)}{\pi^3} E_F \frac{M}{m} \frac{1}{\pi} \int_0^\infty dq^2 \int_0^\pi d\theta \sin^2 \theta L_{skel}^{(\mu)} \left[(2 + \cos^2 \theta) L_I^{(2)} - 3 \cos^2 \theta L_{II}^{(2)} \right]. \quad (26)$$

We have derived and used explicit expressions for the two-loop form factor in Eq. (25) in [10, 35], where we calculated nonrecoil and radiative-recoil correction to HFS in muonium due to the diagrams in Fig. 6. Explicit expressions for the contributions to the energy shifts in Eqs.(2), (26) and (31) from [10] correspond to the integral in Eq. (26) with the three terms on the RHS in Eq. (25) and were obtained without expansion in the small mass ratio. They are rather cumbersome and we will not reproduce them here. Using these expressions we obtain a few leading terms of the expansion in the small mass ratio of the contribution of the diagrams in Fig. 6 to HFS that were calculated earlier

$$\Delta E = \frac{\alpha^2(Z\alpha)}{\pi^3} E_F \left\{ -0.310\,742\,\pi^2 + \frac{m}{M} \left[\frac{3}{4} \ln^2 \frac{M}{m} + \left(\pi^2 - \frac{53}{6} \right) \ln \frac{M}{m} + 7.08072 \right] \right\}. \quad (27)$$

We have checked numerically that the expression in Eq. (26) derived for arbitrary masses reproduces the expansion above in the case of small mass ratio.

In the case of equal masses the contribution of the diagrams in Fig. 6 to HFS reduces to

$$\Delta E_4 = \frac{\alpha^3}{\pi^3} E_F^{Ps} \frac{2}{\pi} \int_0^\infty dq^2 \int_0^\pi d\theta \sin^2 \theta L_{skel} \left[(2 + \cos^2 \theta) L_I^{(2)} - 3 \cos^2 \theta L_{II}^{(2)} \right], \quad (28)$$

where an extra factor 2 before the integral (in comparison with Eq. (26)) arises because we can insert the two-loop electron factor in either of the fermion lines.

After calculations we obtain

$$\Delta E_4 = -3.154\,41\,(1) \frac{\alpha^3}{\pi^3} E_F^{Ps}. \quad (29)$$

D. Light-by-Light Scattering Contribution

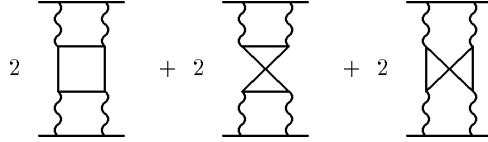


FIG. 7. Diagrams with light-by-light scattering insertions

Due to gauge invariance the light-by-light scattering block fast decreases with the momenta of the external (virtual) photons. Therefore, effectively all integration momenta in the diagrams in Fig. 7 are hard, of order of the electron mass (or in the interval from m to M in the case of unequal masses).

The contribution of the light-by-light scattering block to HFS in the general case of unequal masses has the form [12, 30]

$$\Delta E = \frac{\alpha^2(Z\alpha)}{\pi^3} E_F \frac{3M^2}{32\pi} \int_0^\infty \frac{dq^2}{q^2} \int_0^\pi d\theta \sin^2 \theta \frac{T(q^2, \cos^2 \theta)}{m^2 q^2 + 4M^2 \cos^2 \theta}. \quad (30)$$

The explicit integral representation for the function $T(q^2, \cos^2 \theta)$ and its definition in terms of the light-by-light scattering tensor can be found in [11, 12]. We use in Eq. (30) four-dimensional spherical coordinates introduced above Eq. (3), so q_0 from [12] turned into $q \cos \theta$.

The first terms of the expansion of this contribution to HFS in the small mass ratio were calculated during the years [11, 12, 36, 37]

$$\Delta E = \frac{\alpha^2(Z\alpha)}{\pi^3} E_F \left\{ -0.472\,514\,(1)\,\pi^2 + \frac{m}{M} \left[\frac{9}{4} \ln^2 \frac{M}{m} + \left(-3\zeta(3) - \frac{2\pi^2}{3} + \frac{91}{8} \right) \ln \frac{M}{m} + 5.9949(1) \right] \right\}. \quad (31)$$

We have checked numerically that the general expression in Eq. (30) coincides with the sum in Eq. (31) in the case of small mass ratio.

In the case of equal masses the integral in Eq. (30) reduces to⁵

$$\Delta E_5 = \frac{\alpha^3}{\pi^3} E_F^{Ps} \frac{3}{32\pi} \int_0^\infty \frac{dq^2}{q^2} \int_0^\pi d\theta \sin^2 \theta \frac{T(q^2, \cos^2 \theta)}{q^2 + 4 \cos^2 \theta}. \quad (32)$$

Calculation of this contribution to HFS in positronium proceeds exactly like calculation of the respective nonlogarithmic radiative-recoil correction to HFS in muonium in [12] and we obtain

$$\Delta E_5 = -0.706\,27\,(5) \frac{\alpha^3}{\pi^3} E_F^{Ps}, \quad (33)$$

what coincides with the result first obtained in [20].

E. Two-One Loop Electron Factors

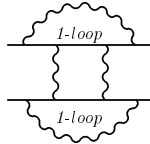


FIG. 8. Diagrams with one-loop radiative photon insertions in both fermion lines

The diagrams in Fig. 8 contain the one-loop fermion factors from Eq. (17) in both fermion lines. Naively, the contribution of these diagrams to HFS can be obtained from the skeleton integral in Eq. (3) by the replacement

$$L_{skel}^{(e)} L_{skel}^{(\mu)} (2 + \cos^2 \theta) \rightarrow \left(\frac{\alpha}{4\pi} \right)^2 \left[(2 + \cos^2 \theta) \tilde{L}_I^{(e)} \tilde{L}_I^{(\mu)} - 3 \cos^2 \theta \left(\tilde{L}_I^{(e)} \tilde{L}_{II}^{(\mu)} + \tilde{L}_{II}^{(e)} \tilde{L}_I^{(\mu)} \right) + \cos^2 \theta (1 + 2 \cos^2 \theta) \tilde{L}_{II}^{(e)} \tilde{L}_{II}^{(\mu)} \right], \quad (34)$$

⁵ There is a misprint in the respective expression in Eq.(14) in [22].

where the terms on the right hand side arise after calculation of the projection of the product of two electron factors (see Eq. (17)) on the HFS structure.

The scalar form factors $\tilde{L}_{I,II}^{(e,\mu)}$ include terms with the scalar form factors $L_A^{(e,\mu)}$ arising due anomalous magnetic moments, see Eq. (18). Therefore, each product of the scalar functions in the square brackets on the right hand side of Eq. (34) contains the term $L_A^{(e)}L_A^{(\mu)}$. As we already mentioned the form factors $L_{I,II}^{(e,\mu)}$ decrease at least as q^2 at $q^2 \rightarrow 0$ relative to the skeleton form factors, while the form factors $L_A^{(e,\mu)}$ behave exactly like the skeleton form factors, see Eq. (20). Hence, each integral of $L_A^{(e)}L_A^{(\mu)}$ is a sum of a linearly infrared divergent and finite contributions, compare with the skeleton integral in Eq. (3). In a more accurate calculation the linearly infrared divergent contribution would be cutoff at the atomic scale $\sim m\alpha$ and would generate a correction of lower order in α . It should be simply subtracted, while we need to preserve the finite part of the integral that generates correction of order $m\alpha^7$. In the general case of different masses (for example, for muonium) the finite part is a recoil contribution and it was calculated in [29]. It is equal to $(9/16)(mM)/(M^2 - m^2)\ln(M^2/m^2)$ up to a normalization factor. Hence, subtraction of the linearly infrared divergent contribution due to terms with $L_A^{(e)}L_A^{(\mu)}$ in Eq. (34) reduces to addition of $(9/16)(mM)/(M^2 - m^2)\ln(M^2/m^2)$ to the respective contribution to HFS instead of all terms on the right hand side in Eq. (34) that proportional to $L_A^{(e)}L_A^{(\mu)}$. After this replacement of the infrared divergent part we obtain a convergent integral with hard characteristic integration momenta in the interval from m to M . The contribution to HFS of the diagrams in Fig. 8 in the case of unequal masses has the form

$$\begin{aligned} \Delta E = & \frac{\alpha(Z^2\alpha)(Z\alpha)}{\pi^3} E_F \left\{ \frac{M}{m} \frac{1}{4\pi} \int_0^\infty dq^2 \int_0^\pi d\theta \sin^2 \theta d\theta \left[(2 + \cos^2 \theta) \right. \right. \\ & \times \left(L_I^{(e)}L_I^{(\mu)} + L_A^{(e)}L_I^{(\mu)} + L_A^{(\mu)}L_I^{(e)} \right) \\ & - 3 \cos^2 \theta \left(L_I^{(e)}L_{II}^{(\mu)} + L_A^{(e)}L_{II}^{(\mu)} - L_I^{(e)}L_A^{(\mu)} + L_{II}^{(e)}L_I^{(\mu)} - L_A^{(e)}L_I^{(\mu)} + L_{II}^{(e)}L_A^{(\mu)} \right) \\ & \left. \left. + \cos^2 \theta (1 + 2 \cos^2 \theta) \left(L_{II}^{(e)}L_I^{(\mu)} - L_A^{(e)}L_{II}^{(\mu)} - L_{II}^{(e)}L_A^{(\mu)} \right) \right] + \frac{9}{16} \frac{mM}{M^2 - m^2} \ln \frac{M^2}{m^2} \right\}. \end{aligned} \quad (35)$$

The first terms of the expansion of the contribution to HFS of the diagrams in Fig. 8 in the small mass ratio are already known for some time [29, 38]

$$\begin{aligned} \Delta E = & \frac{\alpha(Z^2\alpha)(Z\alpha)}{\pi^3} E_F \left[\frac{\pi^2}{2} \left(\ln 2 - \frac{13}{4} \right) \right. \\ & \left. + \frac{m}{M} \left(-\frac{9}{8} \ln \frac{M}{m} - \frac{15}{8} \zeta(3) + \frac{15\pi^2}{4} \ln 2 + \frac{37\pi^2}{24} - \frac{147}{32} \right) + \frac{9}{16} \frac{Mm}{M^2 - m^2} \ln \frac{M^2}{m^2} \right]. \end{aligned} \quad (36)$$

We have checked numerically that in the case of small mass ratio the expression in Eq. (35) coincides with sum above.

In the case of equal masses the integral in Eq. (35) simplifies

$$\begin{aligned} \Delta E_6 = & \frac{\alpha^3}{\pi^3} E_F^{Ps} \left\{ \frac{1}{4\pi} \int_0^\infty dq^2 \int_0^\pi d\theta \sin^2 \theta d\theta \left[(2 + \cos^2 \theta)(L_I^2 + 2L_A L_I) \right. \right. \\ & \left. \left. - 6 \cos^2 \theta (L_I L_{II} + L_A L_{II} - L_A L_I) + \cos^2 \theta (1 + 2 \cos^2 \theta)(L_{II}^2 - 2L_A L_{II}) \right] + \frac{9}{16} \right\}. \end{aligned} \quad (37)$$

After numerical calculations we obtain contribution of the diagrams in Fig. 8 to HFS in positronium

$$\Delta E_6 = -4.739\ 55\ (40) \frac{\alpha^3}{\pi^3} E_F^{Ps}. \quad (38)$$

III. SUMMARY OF RESULTS

We have derived explicit expressions for hard three-loop contributions to hyperfine splitting generated by the six gauge-invariant sets of diagrams with closed electron loops in Figs. 2 - 4 and in Figs. 6 - 8. In the case of unequal lepton masses we confirm numerically the already known results for muonium obtained earlier in the form of an expansion in the small mass ratio. We have calculated the contributions of these diagrams to HFS in the case of equal masses, for positronium. Collecting the results in Eq. (12), Eq. (16), Eq. (24), Eq. (29), Eq. (33), and Eq. (38), we obtain the total hard contribution to HFS in positronium of order $m\alpha^7$ generated by all diagrams with closed electron loops in Figs. 2 - 4 and in Figs. 6 - 8

$$\Delta E = -3.875\ 0\ (4) \left(\frac{\alpha}{\pi} \right)^3 E_F^{Ps} = -1.291\ 7\ (1) \frac{m\alpha^7}{\pi^3} = -5.672\ \text{kHz}. \quad (39)$$

Taking into account all other recent theoretical results [19–21] we obtain the theoretical prediction for HFS in positronium

$$\Delta E_{theor} = 203\,391.89 (25) \text{ MHz.} \quad (40)$$

The latest experimental result is [16]

$$\Delta E_{exp} = 203\,394.2 (1.6)_{stat} (1.3)_{sys} \text{ MHz.} \quad (41)$$

There are no contradictions between theory and experiment at the present level of accuracy, but further reduction of both the experimental and theoretical uncertainties is warranted. Calculation of the remaining ultrasoft and hard nonlogarithmic contributions of order $m\alpha^7$ is the next task for the theory. We hope to report the results for the remaining hard corrections in the near future.

ACKNOWLEDGMENTS

This work was supported by the NSF grants PHY-1066054 and PHY-1402593. The work of V. S. was supported in part by the RFBR grant 14-02-00467.

-
- [1] F. G. Mariam, W. Beer, P. R. Bolton et al., Phys. Rev. Lett. **49**, 993 (1982).
 - [2] W. Liu, M. G. Boshier, S. Dhawan et al., Phys. Rev. Lett. **82**, 711 (1999).
 - [3] K. Sasaki et al., J. of Physics: Conference Series **408**, 012074 (2013).
 - [4] K. S. Tanaka et al., JPS Conf. Proc. **2**, 010405 (2014).
 - [5] M. I. Eides, H. Grotch, and V. A. Shelyuto, Phys. Rep. **342**, 63 (2001).
 - [6] M. I. Eides, H. Grotch, and V. A. Shelyuto, *Theory of Light Hydrogenic Bound States*, (Springer, Berlin, Heidelberg, New York, 2007).
 - [7] P. J. Mohr, B. N. Taylor, and D. B. Newell, Rev. Mod. Phys. **84**, 1527 (2012).
 - [8] M. I. Eides and V. A. Shelyuto, Phys. Rev. Lett. **103**, 133003 (2009).
 - [9] M. I. Eides and V. A. Shelyuto, Phys.Rev. D **80** 053008, (2009).
 - [10] M. I. Eides and V. A. Shelyuto, J. Exp. Theor. Phys. **110**, 17 (2010) [ZhETPh **137**, 24 (2010)].
 - [11] M. I. Eides and V. A. Shelyuto, Phys. Rev. D **87**, 013005 (2013).
 - [12] M. I. Eides and V. A. Shelyuto, Phys. Rev. D **89**, 014034 (2014).
 - [13] A. P. Mills, Jr. and G. H. Bearman, Phys. Rev. Lett. **34**, 246 (1975).

- [14] M. W. Ritter, P. O. Egan, V. W. Hughes, and K. A. Woodle, *Phys. Rev. A* **30**, 1331 (1984).
- [15] A. P. Mills, *Phys. Rev. A* **27**, 262 (1983).
- [16] A. Ishida, T. Namba, S. Asai, T. Kobayashi, H. Saito, M. Yoshida, K. Tanaka, and A. Yamamoto, *Phys.Lett. B* **734**, 338 (2014).
- [17] A. Ishida, talk at the Fundamental Constants Meeting, February 1-6, 2015, Eltville, Germany.
- [18] A. A. Penin, "Testing Quantum Electrodynamics with Positronium State" in proceedings of "Loops and Legs in Quantum Field Theory" PoS LL2014, 074 (2014).
- [19] M. Baker, P. Marquard, A. A. Penin et al., *Phys. Rev. Lett.* **112**, 120407 (2014).
- [20] G. S. Adkins and R. N. Fell, *Phys. Rev. A* **89**, 052518 (2014).
- [21] G. S. Adkins, C. Parsons, M. D. Salinger, R. Wang, and R. N. Fell, *Phys. Rev. A* **90**, 042502 (2014).
- [22] M. I. Eides and V. A. Shelyuto, *Phys. Rev. D* **89**, 111301(R) (2014).
- [23] M. I. Eides, S. G. Karshenboim, and V. A. Shelyuto, *Ann Phys. (NY)* **205**, 231 (1991).
- [24] J. R. Sapirstein, E. A. Terray, and D. R. Yennie, *Phys. Rev. D* **29**, 2290 (1984).
- [25] J. Schwinger, *Particles, Sources and Fields*, Addison-Wesley, Reading, MA, 1973, Vol. 2.
- [26] M. I. Eides, S. G. Karshenboim, and V. A. Shelyuto, *Phys. Lett. B* **229**, 285 (1989); *Pisma Zh. Eksp. Teor. Fiz.* **50**, 3 (1989) [*JETP Lett.* **50**, 1 (1989)]; *Yad. Fiz.* **50**, 1636 (1989) [*Sov. J. Nucl. Phys.* **50**, 1015 (1989)].
- [27] M. I. Eides, H. Grotch, and V. A. Shelyuto, *Phys. Rev. D* **65**, 013003 (2001).
- [28] G. Kallen and A. Sabry, *K. Dan. Vidensk. Selsk. Mat. Fys. Medd.* **29**, 17 (1955).
- [29] M. I. Eides, H. Grotch, and V. A. Shelyuto, *Phys. Rev. D* **70**, 073005 (2004); *ibid.* **88**, 119901(E) (2013).
- [30] M. I. Eides and V. A. Shelyuto, *Phys. Rev. D* **90**, 113002 (2014).
- [31] V. Yu. Brook, M. I. Eides, S. G. Karshenboim, and V. A. Shelyuto, *Phys. Lett. B* **216**, 401 (1989).
- [32] M. I. Eides, H. Grotch, and V. A. Shelyuto, *Phys. Rev. D* **58**, 013008 (1998).
- [33] M. I. Eides, H. Grotch, and V. A. Shelyuto, *Phys. Rev. D* **67**, 113003 (2003).
- [34] M. I. Eides, H. Grotch, and V. A. Shelyuto, *Can. J. Phys.* **83**, 363 (2005).
- [35] M. I. Eides, S. G. Karshenboim, and V. A. Shelyuto, *Phys. Lett. B* **249**, 519 (1990); *Pisma Zh. Eksp. Teor. Fiz.* **52**, 937 (1990) [*JETP Lett.* **52**, 317 (1990)].

- [36] M. I. Eides, S. G. Karshenboim, and V. A. Shelyuto, Phys. Lett. B **268**, 433 (1991); **316**, 631 (E) (1993); **319**, 545 (E) (1993); Yad. Fiz. **55**, 466 (1992); **57**, 1343 (E) (1994) [Sov. J. Nucl. Phys. **55**, 257 (1992); **57**, 1275 (E) (1994)].
- [37] M. I. Eides, S. G. Karshenboim, and V. A. Shelyuto, Phys. Lett. B **216**, 405 (1989); Yad. Fiz. **49**, 493 (1989) [Sov. J. Nucl. Phys. **49**, 309 (1989)].
- [38] N. Kroll and F. Pollock, Phys. Rev. **84**, 594 (1951); *ibid.* **86**, 876 (1952).